Bottom-up Estimation of Stand Leaf Area Index from Individual Tree Measurement Using Terrestrial Laser Scanning Data

Yuzhen Xing, Ronghai Hu, *Senior Member, IEEE*, Hengli Lin, Hong Zeng, Da Guo, Guangjian Yan, *Senior Member, IEEE,* Xiaoning Song, Pierre Kastendeuch, Marc Saudreau, Françoise Nerry, Kai Xue, and Yanfen Wang

***Abstract*—Leaf area parameters are crucial in ecosystem studies. As ecophysiological models advance toward finer detail, accurately estimating LA at various scales becomes essential, particularly for diverse units like urban individual trees. Several algorithms based on terrestrial laser scanning (TLS) data have been developed to obtain the LA of individual trees. However, their use at the stand level needs further research. In this study, the comparative shortest-path algorithm (CSP) is introduced for the automatic individual tree segmentation, thereby facilitating the application of the path length distribution model (PATH) for leaf area estimation at the stand level. Using high-density TLS data, we presented a bottom-up estimation of stand leaf area index (LAI) from 50 individual tree measurements and validated the results at different scales. At the tree scale, the LA derived from TLS and allometric model were highly correlated, with an R-value of 0.83. At the stand scale, the proposed method provides consistent results with the allometric and TRAC instrument measurements, performing better than vertical upward photography. Generally, 23 shared stations under the forest are enough to accurately obtain the LA of 50 trees and the LAI in an urban forest stand. Sensitivity analysis shows that the method is not sensitive to TLS scan resolution and parameters used in tree crown envelope reconstruction. The proposed bottom-up approach provides a new way of estimating the LAI at stand level using TLS and has the advantage of providing multi-level leaf area information and avoiding the scale effect.**

The work was supported by the National Natural Science Foundation of China (NSFC) (Grant No. 42271393, 41901288), Open Fund of State Key Laboratory of Remote Sensing Science (Grant No. OFSLRSS202325), Beijing Nova Program of Science and Technology (Grant No. Z191100001119132), the Youth Innovation Promotion Association CAS, and the Fundamental Research Funds for the Central Universities. *(Corresponding author: Ronghai Hu).*

Y. Xing, R. Hu, H. Lin, H. Zeng, D. Guo, X. Song, K. Xue and Y. Wang are with the College of Resources and Environment, University of Chinese Academy of Sciences, Beijing 100049, China, and with the Beijing Yanshan Earth Critical Zone National Research Station, University of Chinese Academy of Sciences, Beijing 101408, China (e-mail: xingyuzhen20@mails.ucas.ac.cn; huronghai@ucas.ac.cn; linhengli19@mails.ucas.ac.cn; zenghong211@mails.ucas.ac.cn; guoda181@mails.ucas.edu.cn; songxn@ucas.edu.cn; xuekai@ucas.ac.cn; yfwang@ucas.ac.cn).

G. Yan is with the State Key Laboratory of Remote Sensing Science, Faculty of Geographical Science, Beijing Normal University, Beijing 100875, China, and with the Beijing Engineering Research Center for Global Land Remote Sensing Products, Faculty of Geographical Science, Beijing Normal University, Beijing 100875, China (e-mail: gjyan@bnu.edu.cn).

P. Kastendeuch and F. Nerry are with the ICube Laboratory, UMR 7357 CNRS-University of Strasbourg, 300 bd Sebastien Brant, CS 10413, F-67412 Illkirch Cedex, France (e-mail: kasten@unistra.fr; f.nerry@unistra.fr).

M. Saudreau is with the University of Clermont Auvergne, INRA, PIAF, F-63000 Clermont Ferrand, France (e-mail: marc.saudreau@inrae.fr).

Color versions of one or more of the figures in this article are available online at http://ieeexplore.ieee.org

***Index Terms*—Beer's law, bottom-up estimation, clumping effect, leaf area index, path length distribution model, scale effect.**

I. INTRODUCTION

Foliage serves as the dominant control over the vegetation-atmosphere exchanges of mass and energy through photosynthesis, respiration, and transpiration [1-4]. Studies investigating the implications of the terrestrial carbon cycle, species competition, ecosystem, and agroecosystem dynamics, as well as climatological, rely on the fast and accurate extraction of leaf area parameters [5-9]. Leaf area parameters are generally expressed on a horizontal 2D map of leaf area index (LAI) or in a 3D space of foliage area volume density (FAVD) [3, 10, 11]. As the fundamental variable identified by the Global Climate Observing System (GCOS), LAI estimation at various spatial scales from individual trees to the whole terrestrial surface has attracted significant efforts [12, 13].

A key issue in this context is that the LAI estimated at different scales might be inconsistent due to the discrepancies among the sensors and collected data, the clumping effect, spatial heterogeneity of LAI, etc. This problem may be posed as, how can a consistent LAI product be developed from data acquired from a series of sensors that have different spatial resolutions. Considering the LAI definition does not suffer from the scale effect, estimating the leaf area of all individual trees and then calculating the stand LAI based on the LAI definition, which we name as a "bottom-up" approach, may be a new way to understand and solve the scale effect.

At the individual tree scale, the approaches to measure leaf area can be classified into two broad categories: direct and indirect. The direct method involves the counting and measurement of leaves, represented by the methods of destructive sampling and allometry [14, 15]. These typically serve as accurate references to validate results from indirect methods, but are not practical in measuring all trees for a region because they are time-consuming, labor-intensive, and usually destructive [11, 16]. Indirect methods rely on the contact frequency [17] or gap fraction [18] observed by optical instruments to derive stand leaf area parameters. In recent years, passive optical devices such as LAI-2200 [19-22] and digital hemispherical photography (DHP) [23-25] are used to estimate leaf area parameters at an individual tree scale. The

use of these methods needs the input of auxiliary data such as tree crown profile, however, these passive devices themselves cannot provide three-dimensional information to characterize the complex tree crown of an individual tree [3].

As an active remote sensing technology, LiDAR has seen increasingly widespread use to quantify vertical and horizontal canopy structures such as tree height, diameter at breast height (DBH), canopy density, and biomass, because of its fascinating three-dimensional observation ability [26-30]. This has led to efforts to derive more complex and precise leaf area parameters such as individual tree FAVD and vertical FAVD profiles from TLS systems [31, 32].

Currently, four categories of methods have been proposed to estimate the leaf area of an individual tree based on TLS, which are regression-, computer graphic-, contact frequency-, and gap probability-based methods. In the regression-based method, TLS is mainly used to obtain tree dimensions such as tree height and DBH, and then these parameters are substituted into a regression model of tree dimensions and leaf area to obtain an individual tree leaf area [33]. The establishment of the regression model usually relies on manual measurement data of several trees sampled in the forest, which makes the regression-based method inefficient and less portable [34]. Methods based on computer graphic attempt to directly obtain the conversion relationship from discrete points to leaf area[35]. Yun *et al.* [36] utilized the Delaunay triangulation algorithm to construct the scanned leaf surface, and then estimated the leaf area in each layer in combination with the ratio and number of the scanned points. Ma *et al.* [37] developed an approach that directly converts classified points into surface area by considering sampling space, laser incidence angle, and leaf orientation information, leading to estimation of true LAI. Such methods are not affected by clumping effect, but depend on a sufficiently dense and complete point cloud to mitigate occlusion effect. The contact frequency-based method originates from inclined point quadrats theory and typically uses voxels to organize point clouds. Segmenting the canopy into voxels allows for convenient computation of contact frequency in each layer based on the number or empty and non-empty voxels, enabling the description of the vertical foliage profile in tree crowns[38, 39]. In addition, Béland *et al.* [40] proposed the average free path length to calculate the corrected contact frequency and achieved Estimated distribution of leaf area in individuals. This method has also been verified by the maximum likelihood estimation theory[41]. The choice of voxel size in these methods requires more research as it affects the accuracy of the results[7]. Furthermore, such methods usually require multiple scan data for an individual tree, which limits the application efficiency in a real forest. The gap probability-based method relates structural attributes such as the LAI to the gap probability of canopy based on Beer's law, which avoids the influence of the uneven point cloud density or incomplete point cloud of a tree. Calculating the gap probability at the voxel scale based on pulse tracking technology can reduce the clumping effect and extract the leaf area parameters at the voxel scale[42, 43]. However, these methods require more research on the optimal voxel size[3, 44] and how to solve the problems of occluded voxels[45, 46]. Li *et al.* [47] developed a point cloud slicing method based on different incident zenith angle ranges to obtain the true LAI of individual trees. This method retrieves gap fraction using multiple-return information and employs gap size analysis theory to correct the clumping effect. Path length distribution method (PATH) is a gap probability-based method that can be used for estimating the leaf area of an individual tree based on tree crown envelope reconstruction (Hu et al., 2018). This method is efficient, requiring fewer scans, and it thoroughly considers the inequality of path lengths at the tree scale. However, the manual segmentation of the studied tree limits the automation and application of the method in a larger area.

At the stand scale, it is a prevalent idea to extend the direct measurements of individual tree scale to the stand scale by constructing an empirical regression equation. By using the litterfall collection and optical methods, Liu *et al.* [14] estimated the seasonal variation of LAI in four mixed evergreen-deciduous forests. Sirri *et al.* [48] destructively sampled 61 trees to calibrate allometric models suitable for Tropical African broadleaved forests, which was a rare attempt at the estimation of LA and LAI in a tropical forest. These direct and semidirect estimations are inevitably restricted by the representativeness of the sample trees, with high uncertainty and poor portability. Correspondently, due to the developed theory and operational efficient measurement scheme, the optical indirect methods based on the Beer-Lambert law have been invested in more studies [49-51]. The clumping effect is generally recognized as the primary issue causing the underestimation of indirect LAI measurement. As commonly applied methods, finite-length averaging method (LX) [52], gap-size distribution method (CC) [53], combination of the CC method and the LX method (CLX) [54], and path length distribution method (PATH) [55] have provided substantial support for correcting the clumping effect and calculating the true LAI. Relying on the gap size method, Zhu *et al.* [56] eliminated the clumping effect and improved the LAI estimation of 31 forest plots with TLS. Chen *et al.* [57] proposed a method to reduce the clumping effect that occurs within plots and estimate LAI in open-canopy forests using TLS data and PATH. Although correction methods have been proposed and improved constantly, optical indirect methods are still restricted by the clumping effect [58], and especially, it is difficult to consider the disparity of leaf area density among different tree crowns.

This paper proposes a bottom-up approach to estimating stand LAI from individual tree measurements using TLS data and the PATH method. In addition, the influences of unavoidable factors in real forests, such as under-canopy stations, special-shaped canopy envelope, and inter-canopy occlusion, on the results are evaluated to furnish practical guidance for indirect in situ LA measurements on individual trees. The proposed approach will provide a new way of

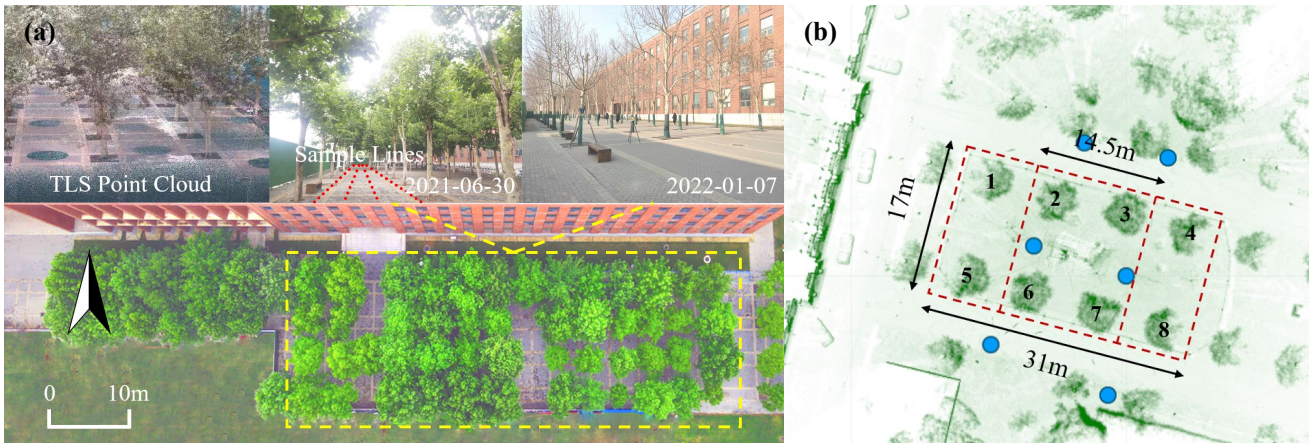

Fig. 1. Overview of the studied trees and acquired data of the study plots. (a) The *Platanus* × *acerifolia* stand. (b) The *Tilia tomentosa* stand.

estimating the LAI at stand level using TLS which has the advantage of providing multi-level leaf area information and avoids the scale effect.

II. Materials

A. Study site

This study includes two distinct experimental sites. The first site is a rectangular woodland about 30 m × 50 m, located in Yanqi Lake campus of the University of Chinese Academy of Sciences (Fig. 1a) (40°24′23″N, 116°40′44″). The woodland is composed of four rows of regularly spaced *Platanus* × *acerifolia* trees with a total number of 50. Each *Platanus* × *acerifolia* tree is approximately 6.5-13.0 m high with an under-crown height of approximately 2.5-3.5 m. The DBH is approximately 0.25 m, and the crown width is approximately 4-6 m.

The second site is a rectangular woodland approximately 17 m × 31 m, located in the historical garden of the University of Strasbourg (Fig. 1b) (48°35′4″N, 7°45′49″E). The woodland consists of two rows of regularly spaced *Tilia tomentosa* trees with a total number of 8. Each *Tilia tomentosa* tree is approximately 9 m high with an under-crown height of approximately 2 m. The DBH is approximately 0.32 m, and the crown width is approximately 5 m.

B. TLS measurement

At the *Platanus* × *acerifolia* stand, TLS data were collected at leafy (June 30, 2021 and July 1, 2021) and leafless (January 7, 2022) periods using a Trimble X7 laser scanner. Specifications of this LiDAR system are shown in Table I. During the leafy period, TLS data from twenty-three scans were collected to shun the loss of features in the point clouds caused by the obstructions among different trees with dense foliage and branches. Similarly, twenty-two TLS scans were collected during the leafless period to eliminate the effect of woody components in the LAI estimation. Point clouds acquired from different stations were registered into the same coordinate system by the automatic register function of the Trimble Perspective software.

At the *Tilia tomentosa* stand, TLS data were collected from six TLS stations using a FARO Focus 3D X330 laser scanner on June 27, 2016. Detailed information on the *Tilia tomentosa* stand and the experimental data were described in Hu *et al.* [32]. For each station, the point cloud was exported to PTX format, which contains the scanner location and information (coordinates and intensity) of all emitted laser pulses regardless of whether the pulses obtain a return or not.

TABLE I
Technical Parameters of the TLS System

Instrument	Trimble X7
Ranging method	Time of flight
Resolution	0.3mrad
Spacing between points	~4mm at 10m
Beam divergence	0.6mrad

C. Allometric measurement and total leaf area estimate

To minimize damage to the trees, a method involving the construction of detailed allometric equation was employed to provide validation values for the leaf area of individual trees. The allometric relationship was established between the leaf area and the length of the shoot, which is the woody element that directly carried leaves [32, 59, 60]. During the leafy period at the *Platanus* × *acerifolia* stand, one hundred and thirty-six shoots of various lengths were randomly sampled from 50 trees, the method adopted in the *Tilia tomentosa* stand[32, 61].

For each shoot, the shoot length, the number of leaves, and the distance between leaf nodes were manually measured by using a measuring tape. All leaves were placed on a piece of A4 size paper used as an area reference and photographed, and then the area of each leaf was extracted through an automatic image processing system, which can identify and measure the leaves on the A4 size paper in the photos. On the basis of these measurements, the allometric statistic of the leaf area and the shoot length was established (Fig. 2). In the constructed allometric equation, the obtained R^2 of 0.94

indicates a robust regression relationship between the leaf area and the shoot length. Therefore, allometric statistics were used to reliably estimate the total leaf area of each tree if the lengths of all branches of each tree is known.

With the help of PCM v2.0 software [62], the branch lengths of all branches of the 50 trees were manually estimated from the 23 high-density point clouds acquired during the leafless period. Then the total leaf area of each tree was obtained according to allometric statistics and used as the reference for comparison with other methods.

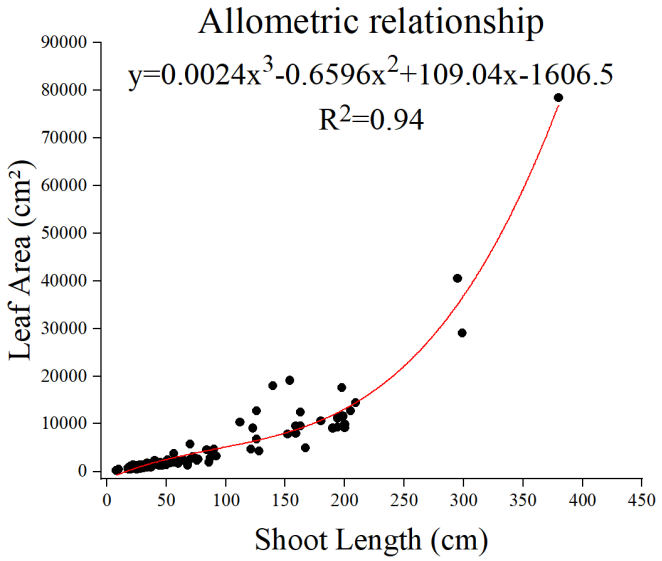

Fig. 2. Allometric relationship between the leaf area and shoot length in *Platanus* × *acerifolia* trees.

D. Leaf angle distribution and G function

Leaf projection coefficient, G, describes the mean projection of a unit foliage area in a particular direction. It can generally be calculated with the leaf inclination angle distribution [63].

The leaf inclination angles of 395 leaves were randomly measured using a protractor in the *Platanus* × *acerifolia* stand at the same time as the TLS data was obtained, that is, on July 1, 2021. Fig. 3 shows the distribution of leaf inclination angles. Then the leaf projection function G can be calculated according to the formula as follows (Fig.3):

$$G(\theta) = \int_0^{\frac{\pi}{2}} A(\theta, \theta_l) g_l(\theta_l) d(\theta_l) \tag{1}$$

$$A(\theta, \theta_l) = \begin{cases} \cos\theta \cos\theta_l, & |\cot\theta \cot\theta_l| > 1 \\ \cos\theta \cos\theta_l \left[1 + \left(\frac{2}{\pi}\right)(\tan\varphi - \varphi)\right], & |\cot\theta \cot\theta_l| \le 1 \end{cases} \tag{2}$$

where $\varphi = \cos^{-1}(\cot\theta)\cot\theta_l$, θ is the viewing zenith angle, θ_l is the leaf zenith angle, and $g_l(\theta_l)$ is the leaf angle distribution.

E. LAI estimate at stand level

Twelve TRAC measurements and 489 vertical upward photographs were used to estimate the LAI of the *Platanus* × *acerifolia* stand as comparison data (Fig. 1). These data were obtained synchronously on June 30, 2021.

TRAC is a maneuverable optical instrument for retrieving LAI by measuring canopy gap size distribution in addition to canopy gap fraction along the sample lines [1, 53]. Twelve TRAC sample lines with a total of 600 meters were acquired, and the regional LAI was retrieved by the TRACWin software [64]. Along the same 12 transects in the test area, 489 vertical upward photographs were taken uniformly at the same height above the ground. The LAI of the stand was obtained as the comparison data by using CC, LX, and CLX methods after preprocessing such as edge clipping and binarization.

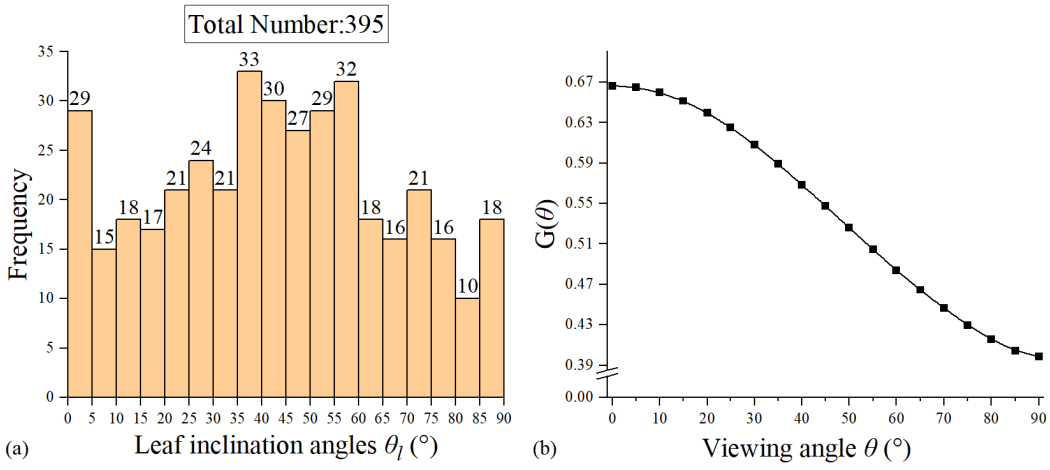

Fig. 3. The leaf inclination angles distribution and leaf projection function in *Platanus* × *acerifolia* trees obtained by measuring 395 leaves. (a) Leaf inclination angles distribution. (b) leaf projection function.

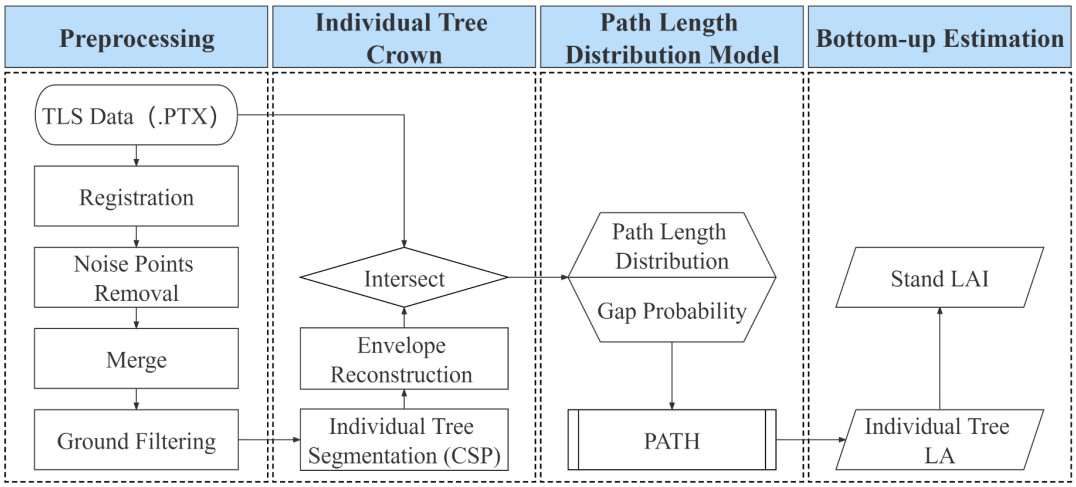

Fig. 4. Workflow of the proposed LAI estimation method using TLS data and the path length distribution model.

III. Methods

In this study, the PATH to TLS data for a single tree was applied to LAI estimation. The workflow of the TLS-based LAI estimation method proposed in this work is displayed in Fig. 4. Firstly, the comparative shortest-path algorithm (CSP)[65] was used to automatically segment individual trees, and then the segmented results were manually trimmed to obtain complete and refined tree crowns. Secondly, the envelope was built for each tree crown using the alpha shapes algorithm [66] and the segmented point cloud. Thirdly, the path length distribution was calculated by simulating the intersection between each emitted laser recorded in PTX files and the envelopes. the gap probability of each tree was then extracted with the number of laser pulses passing through and those entering the tree crown. Fourthly, the path length distribution and gap probability were substituted into the PATH, and combined with the envelope volume to extracted the individual tree LA. Finally, the regional LAI was calculated as the ratio of the sum of all individual trees LA and the area of the experimental plot.

A. Segment Individual trees

Individual tree segmentation is the pre-work of obtaining single tree LA. Although manual segmentation is accurate, its time-consuming and labor-intensive characteristics are not conducive to large-scale data processing. Under the guidance of ecological theories, the CSP algorithm can efficiently segment tree crowns scanned using terrestrial (T)-LiDAR and mobile LiDAR through two steps of trunk detection and subsequent crown segmentation.

After merging point clouds from multiple stations, cropping to obtain the quadrat data, and removing taller non-tree objects such as street lights, the CSP algorithm integrated in the LiDAR360 software (GreenValley, Beijing, China) was applied to preliminarily segment crowns. While the CSP algorithm generally provides stable segmentation results, it is not entirely immune to a small number of segmentation errors. Therefore, the results were restructured to acquire complete and accurate individual crown point cloud data (Fig. 5). This step aimed to facilitate a focused evaluation of bottom-up method during experiments.

B. Envelope reconstruction

As shown in the workflow, an envelope was reconstructed for each individual tree crown by using an alpha shape algorithm (Edelsbrunner and Mücke, 1994) with the help of MATLAB software. This algorithm can build convex and concave envelopes. In the present study, concave envelopes with alpha radius of 0.5 were used to capture the exact shape of the crown points. Additionally, when calculating the gap probability based on single-station TLS, the contours were further refined by removing large gaps at the edges.

C. Path length distribution extraction

The path length distribution was calculated based on all the laser pulses entering the tree crown. For each laser pulse, its path length is defined as the distance between the laser pulse entering and exiting the canopy envelope. Scanning configuration of the TLS (scanning angle range and angle step width) and the original scan file in PTX format was used to simulate the spatial distribution of each emitted laser. Then, each laser pulse was considered to be an infinitely long ray emitted from the TLS, and the intersections between each laser pulse and the envelope of the tree under study were calculated. After filtering out both pulses that do not intersect the envelope and those that intersect the envelope but return in advance due to the object blocking between the research tree and the laser scanner (where the pulse return coordinate is located before the two intersection points between the pulse and the envelope), the path lengths of the remaining laser pulses which enter the tree crown were calculated as the distance between the two intersection points. Finally, the path length distribution was obtained from the statistics of all path lengths.

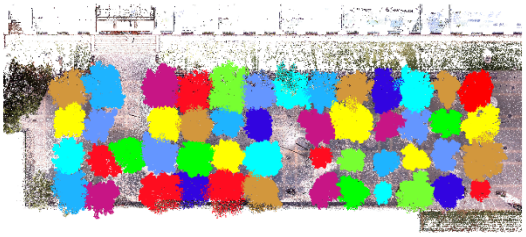

Fig. 5. Individual trees segmentation result at the *Platanus* × *acerifolia* stand using the CSP algorithm (after manual editing).

D. Gap probability calculation

The gap probability was calculated based on all laser pulses that enter the tree crown, which is consistent with the input for the path length distribution. The pulses used have been filtered to exclude those that do not intersect with the crown's envelope or are obstructed before reaching the tree crown, as detailed in Section III.C. In the algorithm implementation, the coordinates of the two intersections between each laser pulse and the envelope were initially calculated. Subsequently, the laser pulses entering the target canopy were categorized into two types based on the relative positional relationship between the pulse return coordinate and the coordinates of the two intersections. Vegetation pulses intersected with vegetation elements and returned within the envelope. The return coordinate of this type is between the two intersections. Penetrating pulses traveled through the tree crown without intersecting with vegetation elements. This type of pulse either did not return, or if it did, the return coordinate was after the two intersections. If the laser pulse return coordinate was before the two intersections, it was the obstructed pulse mentioned earlier and was not included in the calculation. Finally, the gap probability was calculated as the ratio of penetrating pulses to all those entering the tree crown.

E. Path length distribution model

The PATH introduces the path length distribution on the basis of Beer's law to describe the spatial distribution of leaves. The path length distribution function is defined to describe the variation of the path length distribution:

$$p_l(l) = \frac{\hat{p}_l(l)}{\int_0^{l_{max}} \hat{p}_l(l)dl} \tag{3}$$

where l is the path length of the ray that travels through the interior of the canopy and l_{max} is the max path length. $\hat{p}_l(l)$ is the frequency of l falling within the interval $[l, l+dl]$.

When the absolute path length is not available, the relative path length lr is introduced and the path length distribution function is modified as:

$$p_{lr}(lr) = \frac{\hat{p}_{lr}(lr)}{\int_0^1 \hat{p}_{lr}(lr)d(lr)} \tag{4}$$

where $lr = \frac{l}{l_{max}}$. $\hat{p}_{lr}(lr)$ is the frequency of lr falling within the interval $[0,1]$.

Then, the total gap probability canopy P and the LAI within the canopy (LAI_{canopy}) can be expressed as integrals weighted by the path length distribution function:

$$P = \int_0^1 e^{-G\cdot(FAVD\cdot l_{max})\cdot lr} \cdot p_{lr}(lr)\, d(lr) \tag{5}$$

$$LAI_{canopy} = \int_0^1 (FAVD \cdot l_{max}) \cdot cos\theta \cdot lr \cdot p_{lr}(lr) d(lr) \tag{6}$$

where $FAVD$ is the leaf area density. G is the leaf projection function. θ stands for the zenith angle.

Combining with (5) and (6), $FAVD \cdot l_{max}$ is eliminated as a whole. With the support of TLS data, the absolute path length distribution of laser pulses penetrating the tree canopy can be directly extracted and used to separate the path length and leaf area density. In this context, the PATH is modified to accurately retrieve the leaf area density of an individual tree, which is expressed as follows:

$$P = \int_0^{l_{max}} e^{-G\cdot FAVD\cdot l} \cdot p_l(l) d(l) \tag{7}$$

Under the condition that the leaf area density is known, it is only necessary to quantify the crown volume, and then the leaf area of an individual tree can be readily calculated according to the following formula:

$$LA = FAVD \cdot V \tag{8}$$

where LA is the leaf area of a tree, $FAVD$ is the leaf area density, and V is the volume of the tree crown.

F. Weighted mean of the multi-station leaf area density

Affected by factors such as occlusion, the canopy structure information cannot be completely described by the single-station data. Therefore, the leaf area density inversed base on the single-station data has certain limitations. Data from different stations provide structural information of the tree under study at different distances and views. Integrating results from multiple stations is expected to efficiently acquire more stable and accurate estimation. To do this, for each tree, leaf area densities were calculated separately from each station using the PATH, and the results calculated from different sites were averaged using a weighting factor. As the number of effective laser pulses (those used to calculate the path length) most directly reflects the sampling integrity of the tree under study at different stations, and the sum of the path lengths incorporates additional depth information, providing insights into the sampling integrity at the 3D scale. Therefore, the number of effective laser pulses and the sum of path lengths were used as weighting factors for the fusion of the multi-station inversion results. The weighted mean and standard deviation of the leaf area density are expressed as follows:

$$\bar{\rho}_w = \frac{\sum_{i=1}^N \rho_i \cdot w_i}{\sum_{i=1}^N w_i} \tag{9}$$

$$\sigma_w = \sqrt{\frac{\sum_{i=1}^N (\rho_i - \bar{\rho}_w)^2 \cdot w_i}{\sum_{i=1}^N w_i}} \tag{10}$$

where $\bar{\rho}_w$ is the weighted mean of the leaf area density, σ_w is the weighted standard deviation, ρ_i is the leaf area density that was calculated from each station, and w_i is the weighting factor.

G. Leaf and woody areas

Since the leaf and woody components are simultaneously recorded by laser scanner during the leafy period, the path length distribution method provided the sum of leaf area and

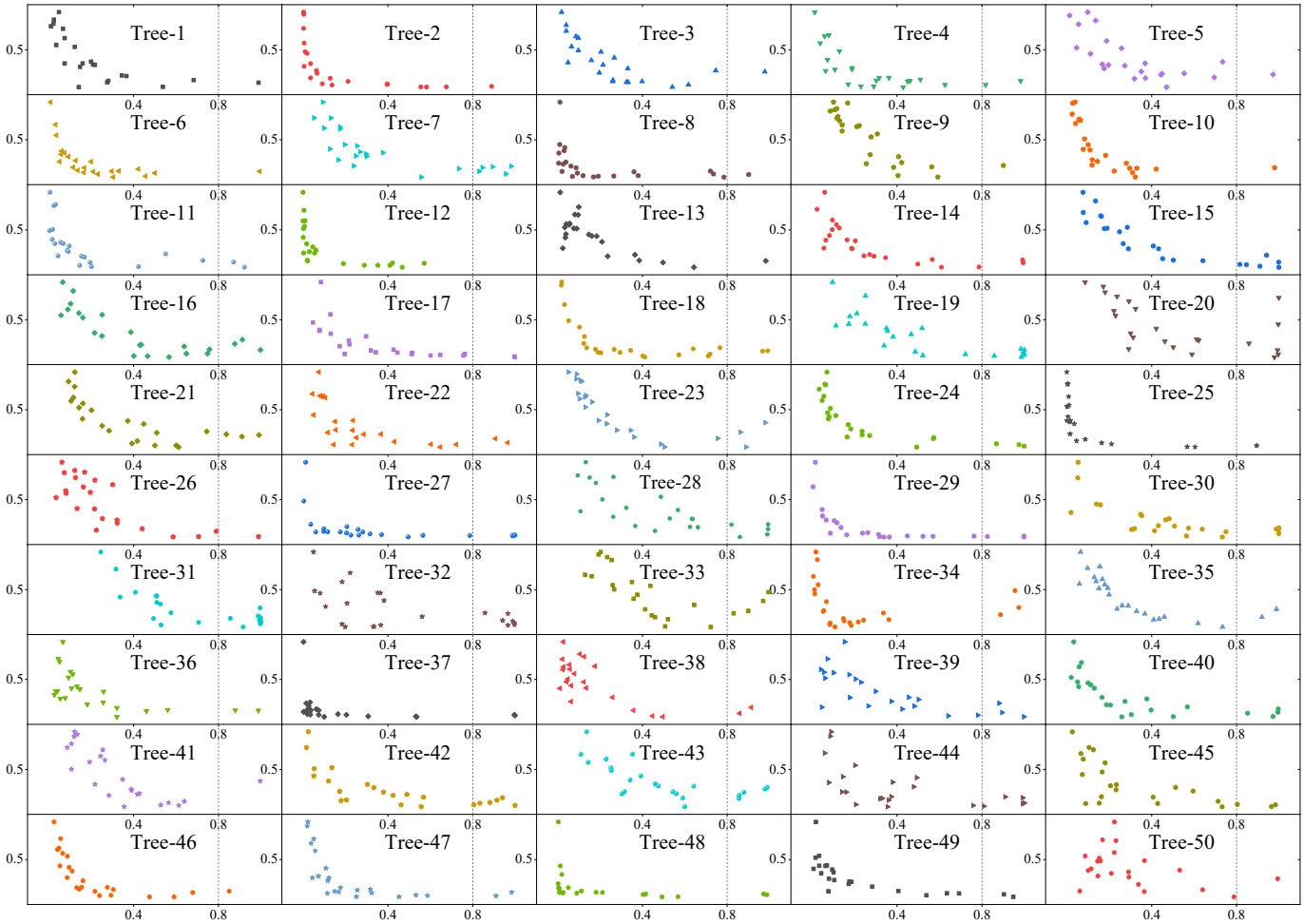

Fig. 6. The relationship between the FAVD (normalized) of individual *Platanus* × *acerifolia* trees at different stations and station visibility rate. Among them, the dotted lines indicate where the visibility rate = 0.8 is located.

woody area (WA), which is called the plant area (PA). This had a different physical meaning from the leaf area directly provided by the allometric method, resulting in no direct comparability between the two results. Therefore, the point cloud data of leafless period were used to calculate the woody area using the same model used during the leafy period. Finally, the leaf area (LA) of the PATH is expressed as follows:

$$LA = PA - WA \tag{11}$$

where PA is the result of the PATH during the leafy period, and WA is the result of the PATH during the leafless period.

H. Evaluation method

Consistency of the leaf area parameters at individual level was accessed using allometric methods and the leaf area index at the stand level was assessed by inter-comparison among TLS estimation, allometric measurement, TRAC measurement and vertical upward photography. Comparisons between the reference and estimated leaf area parameters are expressed in terms of pearson correlation coefficient (r), root mean square error (RMSE) and normalized RMSE.

$$r = \frac{\sum_{i=1}^{n}(x_i-\bar{x})(y_i-\bar{y})}{\sqrt{\sum_{i=1}^{n}(x_i-\bar{x})^2}\sqrt{\sum_{i=1}^{n}(y_i-\bar{y})^2}} \tag{12}$$

$$RMSE = \sqrt{\frac{\sum_{i=1}^{n}(x_i-y_i)^2}{n}} \tag{13}$$

$$nRMSE = \frac{RMSE}{y_{max}-y_{min}} \tag{14}$$

where x_i and y_i are the estimated (TLS result) and measured (allometric result) values for sample i, respectively, n is the number of samples, $\bar{x}$ is the mean of estimated values, and $\bar{y}$, y_{max} and y_{min} are the mean, max, and min of measured values, respectively.

IV. Results

A. The result from different stations and the weighted mean result of all stations

For each tree, the leaf area density is retrieved from different TLS stations separately, and the weighted mean of the different stations is calculated using (9). The result show that visibilities of the same tree from different stations, which is calculated as the ratio of the number of laser pulses reaching the tree crown envelope and the number of laser pulses emitted towards the tree crown envelope (Hu et al., 2018),

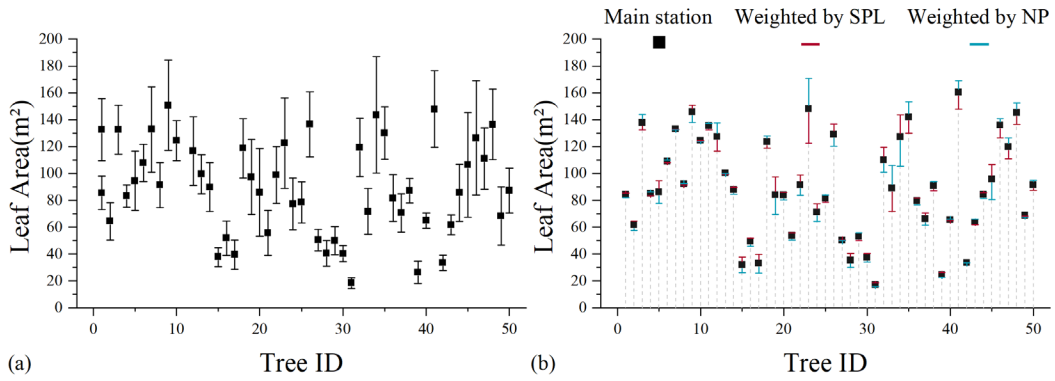

Fig. 7. Weighted impact of different stations results at the *Platanus* × *acerifolia* stand. (a) The weighted mean and weighted standard deviation of all station results for the fifty trees. (b) The results of the best observation stations and the weighted results of all stations when the number of effective laser pulses is used (NP) or the sum of path lengths (SPL) are used as weighting factors.

vary dramatically from 0 to 100% and there are very few stations with visibilities higher than 80% (Fig. 6). The results of stations with little visible proportions (generally less than 20%) are generally higher than the weighted mean of all stations results and volatile. With the increase of visible proportion, the retrieval of individual station approaches the weighted mean and the stability rapidly improves. The relative proportion of the weighted standard deviation to the weighted mean of 23 stations results for the fifty *Platanus* × *acerifolia* trees ranged from 8.8% to 37.9% (Fig. 7a). The relative proportion of the weighted standard deviation to the weighted mean of 6 stations results for the eight *Tilia tomentosa* trees ranged from 3.2% to 15.4%. Considering these results from both study sites, it is showed that this method can consistently and reliably characterize various plant areas with low standard deviation for different forest types and tree species.

For each tree, the station with the largest sum of path lengths is selected as the main station, which usually has both the highest visibility and the largest number of lidar pulses entering the canopy synchronously because of the best observation conditions such as being closer to the canopy and less blocks in front of the canopy. The leaf area of each tree was estimated by three means, including using the best observation stations, using all stations with the number of effective laser pulses as weighting factors, and using all stations with the sum of path lengths (SPL) as weighting factors. The three results are consistent for most trees. However, in a few trees, we have observed the disunity of the three means (Fig. 7b). This may be related to the asymmetry of the observed tree crown, which is consistent with the direct observations. The average leaf area density weighted by the number of pulses and by the sum of path lengths are both consistent with the result of the main station (Fig. 7b), thereby indicating that either number of pulses or the sum of path lengths is a favorable weighting factor.

B. Woody-to-total area ratio

With the total path lengths as the weight, the leaf area density of each individual tree was calculated by weighted average of the results from multiple stations, then the leaf area density was converted into leaf area by (11) to facilitate subsequent analysis. Both the wood and leaf points in the leafy period data contribute to the retrieve results so that the result of the method based on Beer's law at the leafy period is the plant area. Meanwhile, the result in winter when all the leaves have fallen is assumed to represent the woody area for both the leafless and leafy periods. Therefore, based on the data of

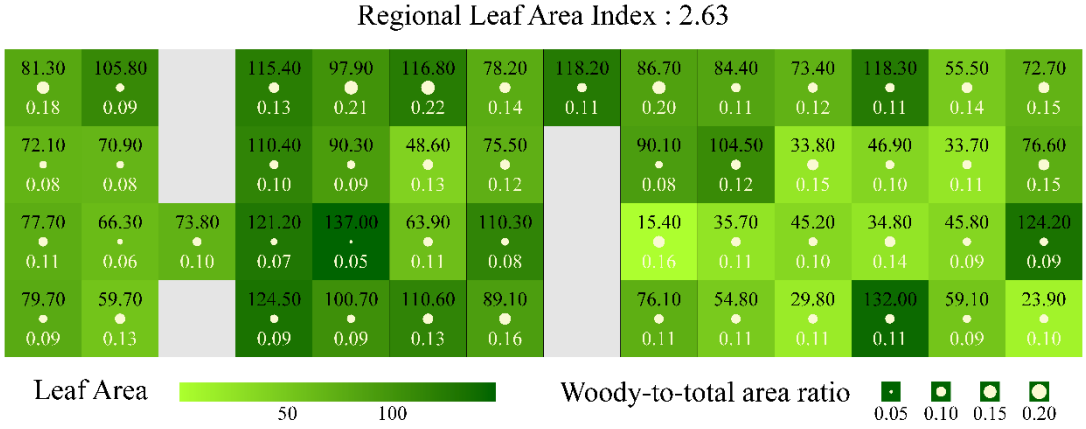

Fig. 8. The spatial heterogeneity distribution of individual trees leaf area (black numbers above the circles) and woody-to-total area ratio (white numbers below the circles) at the *Platanus* × *acerifolia* stand.

leafy and leafless periods, the path length distribution model is used consistently to retrieve the plant area and woody area of the researched trees (Fig. 8). The effect of non-photosynthetic components on LAI measurements can be described by the woody-to-total area ratio, that is, the ratio of woody area to plant area. Of the fifty *Platanus* × *acerifolia* trees considered in this study, the woody-to-total area ratio ranged from 0.05 to 0.22 with the average of 0.12 and the standard deviation of 0.04 (Fig. 9). This result agrees well with a previous study wherein the mean woody-to-total area ratio of four *Platanus* × *acerifolia* trees manually measured by Baptista *et al.* [67] was 0.11. This also indirectly verifies the reliability of the model used in this paper and the accuracy of the results.

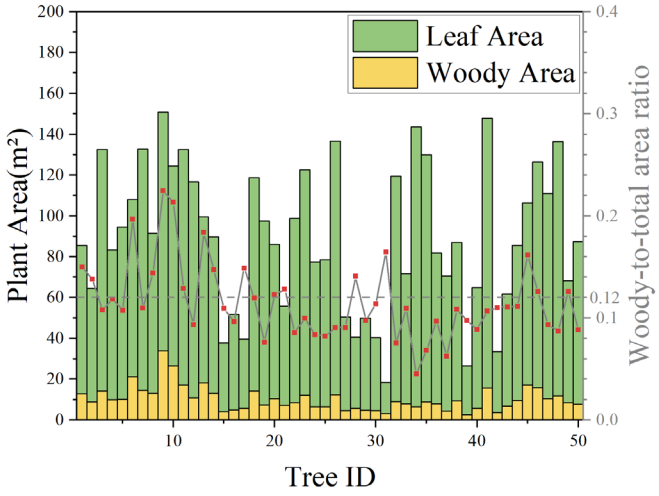

Fig. 9. The plant area, leaf area and woody area of fifty individual *Platanus* × *acerifolia* trees. The dot chart indicates the Woody-to-total ratio of different individual tree, and the dotted line points to the average Woody-to-total ratio of 50 trees.

C. Leaf area of individual trees

At the *Platanus* × *acerifolia* stand, the TLS-based "true" leaf area of fifty individual trees were successfully calculated from the plant area and woody area according to (11) and then compared with ground leaf area measurements determined by allometric statistics (Fig. 10). The leaf areas of the fifty trees ranged from 15.44 m^2 to 137.00 m^2. Estimates of the LA of fifty trees derived from TLS and allometric measurements were moderately correlated, with an r value of 0.66 and an nRMSE value of 0.19 (Fig. 10a). It can be seen intuitively that the four points with large deviations cause great disturbance to the results. After eliminating these four points which are seriously suspected to be outliers, a significant improvement was obtained with an r value of 0.83 and an nRMSE value of 0.13. Results show TLS-based leaf area estimations were strongly correlated with the allometric statistics leaf area measurements when very few outlier points were ignored (Fig. 10a). The existence of very few outlier points will be discussed and analyzed later. The LA estimated using the TLS main station with the maximum visibility alone, weighted by SPL, and weighted by NP are generally consistent (Fig. 10b).

At the *Tilia tomentosa* stand, the estimated leaf area for tree 3 is 189.97 m^2, showing a high consistency with the allometric measurement results (leaf area: 183.24 m^2, plant area: 229.24 m^2 and woody-to-total area ratio: 0.2). After correcting for the impact of the woody components based on the woody-to-total area ratio of 0.2 obtained from the verification value of tree 3, the leaf area of the eight *Tilia tomentosa* trees ranges from 153.15 to 190.50 m^2. The weighted standard deviation among the results from 6 stations for the eight trees ranged from 3.2% to 15.4%, with the results from main stations closely aligning with the weighted results. Due to the non-specialized station layout, trees 1 and tree 8, located at the edge of the study site, have incomplete outlines. Although the FAVD inverted from different stations is stable and credible, incomplete outline leads to an underestimation of the canopy volume, thereby underestimating the individual tree leaf area. To address this,

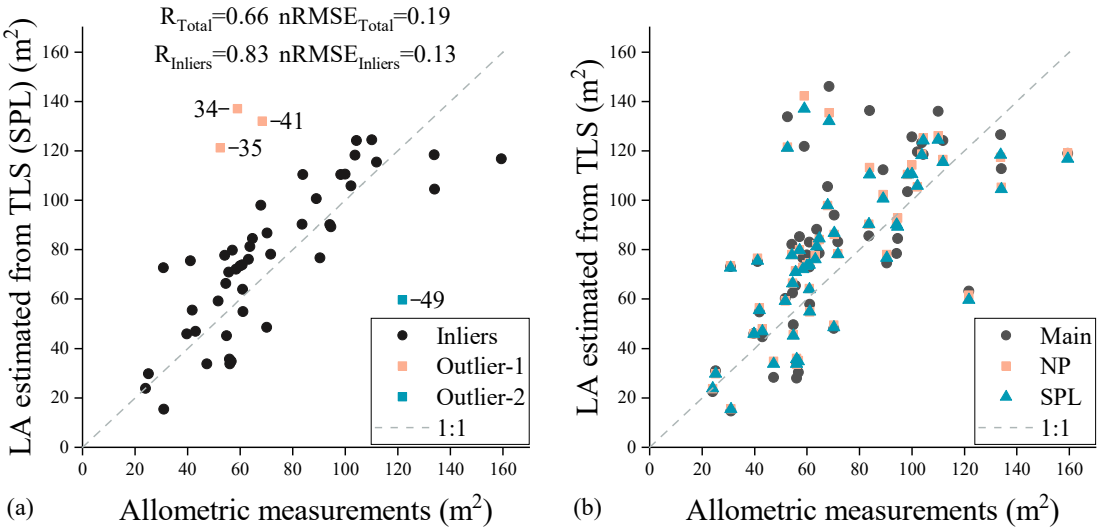

Fig. 10. Comparison of individual tree leaf area between TLS data inversion and allometric measurements at the *Platanus* × *acerifolia* stand. The points identified in color are considered as outliers.

we estimated the volume underestimated proportions of these two trees (tree 1: 0.33, tree 8: 0.20) and corrected their leaf area accordingly: tree 1 (154.13 – 230.04 m^2) and tree 8 (190.50 – 238.12 m^2).

D. Leaf area index of the experimental area

The LAI of the *Platanus* × *acerifolia* stand was calculated using the TLS, allometric statistics, TRAC and vertical upward photographs data respectively. Four mainstream methods were used to correct the clumping effect of the result retrieved with vertical upward photographic data, they are the PATH, CC, LX, CLX methods. The woody components and leaves could not be directly separated in the TRAC and vertical upward photographs data, for this reason, the five results based on these two types of data were corrected using the woody-to-total area ratio (0.12) extracted by TLS result to obtain the true leaf area indexes. In Fig. 11 the final LAI results based different data and methods are presented. No great difference in LAI is observed among the different results. In particular, the estimate from TLS (weighted by SPL or NP) is in a good agreement with that from TRAC, which is considered the standard for estimating LAI, and the absolute errors between them and the estimate from allometric statistics are 0.24 and 0.26 respectively. At the stand scale, the estimations of the TLS main station with the maximum visibility alone (2.72), weighted by SPL (2.63) and weighted by NP (2.66) shown high consistency. The four estimates based on vertical upward photographs data show consistent underestimation compared to the estimate from allometric statistics. Severe occlusion effect and inability to accurately distinguish between the sky and plants materials due to direct sunlight and shadow are two possible causes in 2D images.

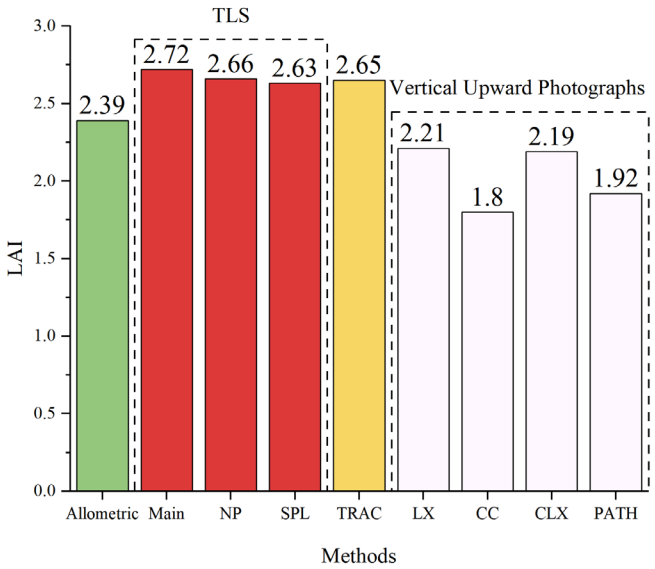

Fig. 11. Comparison of the LAI retrieved from different data and methods at the *Platanus* × *acerifolia* stand.

By combining the quadrat area of 246.5 m^2 with the leaf area of four trees (trees 2, 3, 6, and 7) that have complete outlines (864.71 m^2), the inverted LAI of the *Tilia tomentosa* stand is 3.51. Compared to the allometric result of 3.65 from the urban tree database[68, 69], the difference is 0.14, and the relative error is 3.91%. Considering all eight trees, the quadrat area is 527 m^2, and the LAI allometric result is 3.27. Initially, TLS estimated a value of 2.64. After correcting the leaf area of tree 1 and tree 8 with incomplete outlines, the final stand LAI is 2.87 indicating a deviation of 0.4 and a relative error of 12.3% when compared to the allometric result.

E. Estimations under different parameter settings

The estimation of individual tree leaf area depends on accurately obtaining the gap probability and path length distribution within the target tree canopy. In this process, data quality parameters represented by scanning resolution and envelope construction parameters represented by alpha radius are involved. To thoroughly investigate the influence of different parameter settings on leaf area estimation, controlled variable experiments were conducted within the *Platanus* × *acerifolia* stand.

Scanning resolution is a crucial indicator for characterizing TLS data quality, and also reflects the efficiency of data acquisition. To analyze the influence of scanning resolution on leaf area estimation, the original point cloud with an angular resolution of 0.3 mrad was subsampled at intervals of 2, 3 and 4 points. Subsequently, TLS datasets with angular resolutions of 0.6, 0.9 and 1.2 mrad were constructed. The same method and process were applied to estimate the leaf area based on the TLS data at different resolutions. The three experiments with resolutions of 0.6 mrad, 0.9 mrad and 1.2 mrad were conducted simultaneously for individual tree segmentation, thus the differences in leaf area estimation were only caused by the variations in scanning resolution. The envelopes reconstructed from the TLS data at different resolutions show nearly no difference. In comparison to 0.6 mrad result, the average relative errors of leaf area for 50 individual trees at resolution of 0.9 mrad and 1.2 mrad were 2.52% and 4.24%. Compared to the 0.3 mrad result, the average relative errors in the three experiments (0.6 mrad, 0.9 mrad, and 1.2 mrad) were 4.01%, 4.55%, and 4.60%, respectively. These errors resulted from differences in both scanning resolution and the outcomes of individual tree segmentation. At the stand scale, the LAI inverted from the data at four resolutions was 2.63, 2.60, 2.62 and 2.67, respectively. In general, scanning resolution demonstrated minimal impact on leaf area inversion.

The alpha radius (r) is the core parameter of alpha shape algorithm. Based on the original r=0.5, adjustments were made only to alpha radius=0.3, 0.4, 0.6, and 0.7 to consider the impact of envelope construction parameters on inversion results. With the increase of r, the envelope volumes of individual trees exhibit a consistent rise. As r increased from 0.3 to 0.7, the average envelope volume of 50 individual trees increased by 70.55%, while the corresponding average relative error of leaf area was only 8.74%. Compared with the results obtained when r is set to 0.5, the average relative errors of leaf area at r values of 0.3, 0.4, 0.6, and 0.7 are 7.12%, 4.03%, 2.81%, and 4.24%, respectively. While the envelope volume undergoes significant changes with varying values of r, the inversion results for leaf area remain remarkably stable.

V. Discussion

A. Consistency of leaf area by PATH and allometric model

Although a good allometric equation of branch length with leaf area for *Platanus* × *acerifolia* trees has been obtained, it is undeniable that the allometric result itself has certain errors for individual trees with variability. It took nearly a month to accurately measure the length of all branches in the point cloud data, but the measurement error is still unavoidable, especially at the top of the tree crown where the point cloud was considerably missing. The four suspected outliers within the *Platanus* × *acerifolia* stand can be divided into two categories, among which the TLS estimates of the three trees numbered 34, 35, and 41 are significantly higher than those of the allometric results. The common problem of the three trees is that the canopy is irregular. There are unique branches at the lower part of the canopy that protrude from the entire canopy and form a joint sub-canopy (Fig. 12). Meanwhile, a station (usually is the main station) is set just below the sub-canopy, and the result of this station are significantly higher than other stations. The internal reason may be that the sub-canopy is too close to the scanner, so that the gap probability is obviously underestimated. At the same time, we use a finer concave envelope and remove the large gap at the edge of the envelope, which inadvertently amplifies the effect of locally shorter path lengths, further exacerbating the overestimation of FAVD. Using a relatively rough concave envelope may be an effective solution. The concave envelope makes the canopy become a whole again, which eliminates the underestimation of the gap probability caused by the perspective scanning. Table II shows that the results of convex envelope are rough but stable, while the result of the refined concave envelope are precise but more sensitive to the special-shaped crown, which may lead to an overestimation.

TABLE II
Differences in the LA Results of Using Convex and Concave Envelopes for Special-Shaped Crowns of *Platanus* × *acerifolia* Trees

Tree ID	Allometric (m²)	Concave (m²)	Convex (m²)
34	59.1	137.0	86.9
35	52.5	121.2	78.5
41	68.4	132.0	44.7

One observation is that the upper branches of the experimental *Platanus* × *acerifolia* trees had a more pronounced tendency to grow upwards, rather than emanating more lateral branches. This characteristic would lead to an overestimation of LA when finely measuring the upper branches. The upward growth trend of the tree numbered 49 is more obvious, which is not limited to the upper part of the canopy. At the same time, the point cloud of the upper part of this tree is very complete, and the number of branch measurements is the largest (163) among the 50 trees (ranging from 32 to 163, the average is 78). The allometric result of the tree numbered 49 is nearly twice as high as for several trees with the same approximate envelope volume (Table III). This evidence suggests that the error of the *Platanus* × *acerifolia* tree numbered 49 comes from a significant overestimation of the allometric result rather than an underestimation of TLS method.

TABLE III
Basic Information of the *Platanus* × *acerifolia* Tree Numbered 49 and Trees with Approximate Same Envelope Volumes

Tree ID	Volume (m^3)	PATH (m^2)	N_b	Allometric (m^2)
05	86.9	84.4	91	64.8
49	92.0	59.7	163	121.8
36	92.1	73.7	89	60.9

N_b number of branch measurements

B. Consistency of LAI by using the different data and method

Our analysis showed that LAI estimate at the *Platanus* × *acerifolia* stand from TLS was in good agreement with that from TRAC which corrects clumping effect and provides the true LAI. The allometric result and vertical upward photographs result are also used as references. In spite of the drawbacks of these methods, we show that these very different techniques generated similar results, indicating that the TLS methods show a high degree of robustness (Fig. 11). The results from the vertical upward photographic data show a consistent underestimation as reported in many previous studies (Fig. 11). There are three possible reasons for the underestimation. First, in 2D images, the problem of occlusion is more noticeable than with TLS. Second, some photos were taken in direct sunlight so that the plant materials are difficult to be differentiated from the sky, which may cause an overestimation of the gap probability and thus significant underestimation of LAI. Otsu method [70] was applied in this study to improve the accuracy of results, especially in comparison with single manual thresholding. Nonetheless, some errors could still be detected in the images. Third, the degree of closeness between the G-value used in the model and the real G-value at a specific shooting angle affected LAI extraction accuracy. The mean G-value (0.66) of the 0-15°angles was used, which does not rule out an underestimation of the LAI caused by this value being higher than the true G value.

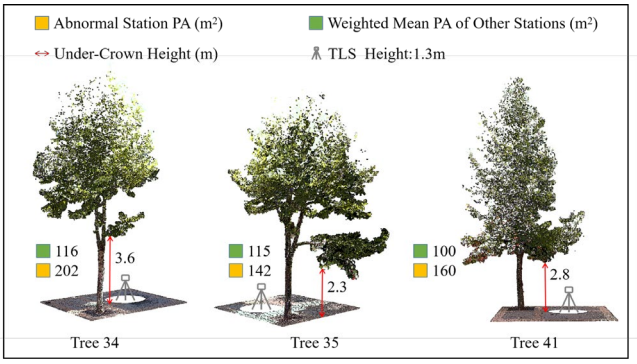

Fig. 12. Schematic diagram of abnormal tree crown and lidar station location.

C. Consistency of using the leaf area density and path length distribution

Different from most previous studies, this study did not set up multiple favorable observation stations for individual trees, but placed enough shared stations within the the *Platanus* × *acerifolia* stand to cover all study trees. This method is closer to the real application scenario, but it also faces many challenges. For each tree, only a few stations with unobstructed views can provide the overall path length distribution and gap probability of the studied tree, which corresponds to a high confidence result. The vast majority of stations are blocked in varying degrees. The uncertainty of path length distribution and gap probability obtained by these blocked stations increases, which leads to a decrease of the consistency of results from different stations. When the occlusion is further increased, it is almost impossible to obtain the point cloud of the studied tree through the block by multiple canopies, but since the TLS height is usually lower than the bottom of the canopy, it is still possible to obtain the lower layer point cloud of the studied tree. Direct observation shows that the proportion of woody components at the bottom of the canopy is higher, and the large gap at the edge of the envelope is removed when the envelope is refined, so that the results of these stations are significantly higher than the average of all stations. The retrieval of different stations is rapidly stable with the improvement of visibility (Fig. 6). Another interesting phenomenon observed in Fig. 6 is that there is usually a rise at the end of the FAVD-Visibility curve when there are multiple stations with a visibility rate close to 100% for an individual tree. This phenomenon is considered to be caused by the distance between the lidar station and the tree crown. LiDAR is a kind of perspective scanning, and a two-dimensional gap is used in this study. This may lead to underestimation of the gap probability in cases where the scanner is too close to the crown, special-shaped crowns, and used too fine concave envelope.

Visibility is a potential index for screening effective stations. Although several of these results would enlarge the weighted standard deviation, we considered the results of all stations. The use of weighted mean demonstrates the following advantages despite the feasibility of filtering the data with low reliability: consistency, universality, and efficiency. At the *Platanus* × *acerifolia* stand, with the introduction of sum of path lengths as a weighting factor, the contribution of the main station was approximately 7.8%-72.3%, and the contribution of stations which visibility below 20% was only approximately 1%. All of these indicate that through the weighted average, the data of all stations were efficiently considered, and the uncertainty of the low-confidence stations to the weighted mean was largely limited. Meanwhile, the LA of each tree and the LAI of the stand estimated using only the main station is consistent with that weighted by the number of pulses or by the sum of path lengths in this study (Fig. 10b, 11). The reason is that the visibility of each tree is above 80% using only the main station, with 23 scans in an urban forest containing 50 trees. It indicates using the main station alone might be enough to characterize the LA of individual tree and the LAI of the plot if the visibility of each tree from the main station reaches a certain standard. The 23 scans set in the *Platanus* × *acerifolia stand* might be sufficient but redundant for characterizing au urban forest of 50 trees, and the minimum required number of scans could be studied in the future.

The TLS stations layout at the *Tilia tomentosa* stand were not specifically tailored for the selected experimental area, resulting in only one-sided observational point cloud for several trees located at the edge of the study site. This narrow observation condition posed limitations in obtaining the complete outline of the tree crown. The weighted standard deviations for four trees (tree 1, 4, 5 and 8), affected by incomplete outlines, range from 9.45% to 15.41%. The relatively low standard deviations indicate that the FAVD inversion from different stations remain relatively stable under conditions of incomplete outlines. However, incomplete outlines can lead to an underestimation of canopy volume, thereby underestimating individual tree leaf area and stand LAI. Therefore, when deploying TLS stations, the relative positions of the stations should still be considered to ensure the acquisition of complete outlines of the target canopies. Typically, achieving this is not difficult. It requires having 2-3 stations among the shared stations capable of capturing the complete outlines for the target tree crown. It's worth noting that it is recommended to set up stations outside the experimental site to obtain complete tree crown outlines for trees located at the edges.

D. Parameter sensitivity analysis

The TLS scanning resolution affects leaf area estimation from two aspects: path length distribution and gap probability. Under different scanning resolutions, extremely small differences between envelopes basically only occur at the edges. The path length distribution is determined by the envelope shape, so the path length distribution is not sensitive to the TLS resolution. The envelope is composed of triangular patches, with more gaps clustered around the edges. As the scanning resolution decreases, the sampling at the edges decreases, and the resulting gap probability fluctuation may be a direct source of inversion uncertainty. The average relative error of 50 individual *Platanus* × *acerifolia* trees at 0.3 and 1.2 mrad resolution is relatively small (4.60%), indicating that the method is not sensitive to scanning resolution, which is positive for large-area forest estimation. In large-area forest estimation, using relatively low-resolution settings and more stations may be a more practical observation strategy. Relatively low resolution is conducive to improving data collection efficiency, while more stations facilitates obtaining the complete outline of the tree crown and improving the stability of individual trees inversion.

According to the principles of the alpha shape algorithm, a decrease in the alpha radius results in tighter generated envelopes, leading to a reduction in the consistency of envelope volume. As the envelope tightens, the gaps at the edges gradually disappear. The path length distribution is

insensitive to these changes, while the gap probability estimation increases, resulting a corresponding rise in the FAVD estimation. This offsetting effect significantly mitigates the impact of volume changes. The average relative error of 50 individual *Platanus* × *acerifolia* trees remains relatively small (8.74%) when alpha radius is set to 0.3 and 0.7, indicating that the method is not sensitive to the alpha radius. Furthermore, comparisons with the result when alpha radius is 0.5 (average relative errors: 0.3: 7.12%, 0.4: 4.03%, 0.6: 2.81%, 0.7: 4.24%) reveals that within a certain range, a larger alpha radius, i.e., a relatively loose envelope, can provide more stable inversion results. Therefore, the recommended alpha radius values are 0.5 and 0.6.

VI. Conclusions

An efficient and automatic method is proposed to estimate the individual tree leaf area in forest areas. By this method, we realize bottom-up estimation of forest-stand level LAI based on individual tree leaf area. By comparing TLS estimates with allometric equation measurements, this study demonstrated that not specialized but regional TLS data can provide statistically similar true LA estimates of individual trees (r = 0.83, nRMSE = 0.13, after removing 4 outliers). Due to the mutual occlusion between tree crowns, there are great differences in the observation capacity of different stations. Visibility is a potential index for screening effective stations. The retrieval of different stations rapidly stabilizes with the improvement of visibility. Moreover, the weighted average of the results of all stations with the sum of path length or the number of pulses as weighting factors is an efficient and stable method. The canopy envelope has an impact on the inversion results. Specifically, the refined concave envelope is beneficial for more accurate results. However, the result of the convex envelope exhibits better stability in complex cases such as special-shaped canopy. At the *Platanus* × *acerifolia* stand, the results of the proposed method are consistent with the allometric measurement and TRAC instrument measurement (Allometric:2.39 $m^2 \cdot m^{-2}$, TLS:2.63 $m^2 \cdot m^{-2}$, and TRAC:2.65 $m^2 \cdot m^{-2}$). Generally, 23 shared stations under the forest are enough to accurately obtain the LA of 50 individual trees and the LAI in an urban forest stand. Consistent results in the *Tilia tomentosa* stand demonstrate the generality and applicability of the method to different forest types and tree species. The proposed bottom-up approach provides a new way of estimating the LAI at stand level using TLS. It has the advantage of providing multi-level leaf area information and avoiding the scale effect, showing great potential in the study of spatial heterogeneity of LAI, tree competition, and forest spatial structure. The application of this method to airborne LiDAR for large-scale observations and the further exploration of acquiring the 3-D distribution of leaf area density within individual trees remain two significant directions for future efforts.

Acknowledgment

The authors sincerely thank the research team led by Cheng Wang from the Aerospace Information Research Institute of the Chinese Academy of Sciences for providing the PCM v2.0 software, and Beijing GreenValley Technology Company for the LiDAR360 software. Both tools greatly facilitated our data preprocessing. The authors also appreciate the efforts of Zuopei Zhang, Boyang Ding, and Beiang Chen who contributed to the allometric measurements.

References

[1] J. M. Chen, "Optically-based methods for measuring seasonal variation of leaf area index in boreal conifer stands," *Agricultural and Forest Meteorology,* vol. 80, no. 2-4, pp. 135-163, 1996.

[2] H. Ren, G. Yan, R. Liu, F. Nerry, Z.-L. Li, and R. Hu, "Impact of sensor footprint on measurement of directional brightness temperature of row crop canopies," *Remote Sensing of Environment,* vol. 134, pp. 135-151, 2013.

[3] S. Wei, T. Yin, M. A. Dissegna, A. J. Whittle, G. L. F. Ow, M. L. M. Yusof, N. Lauret, and J.-P. Gastellu-Etchegorry, "An assessment study of three indirect methods for estimating leaf area density and leaf area index of individual trees," *Agricultural and Forest Meteorology,* vol. 292-293, pp. 108101, 2020.

[4] D. L. B. Jupp, D. S. Culvenor, J. L. Lovell, G. J. Newnham, A. H. Strahler, and C. E. Woodcock, "Estimating forest LAI profiles and structural parameters using a ground-based laser called 'Echidna(R)," *Tree Physiology,* vol. 29, no. 2, pp. 171-181, 2008.

[5] D. D. Baldocchi, and P. C. Harley, "Scaling carbon dioxide and water vapour exchange from leaf to canopy in a deciduous forest. II. Model testing and application," *Plant, Cell and Environment,* vol. 18, no. 10, pp. 1157-1173, 1995.

[6] G. G. Parker, "Structure and microclimate of forest canopies," *Forest canopy*, pp. California, USA, pp. 73–106., 1995.

[7] M. Béland, D. D. Baldocchi, J.-L. Widlowski, R. A. Fournier, and M. M. Verstraete, "On seeing the wood from the leaves and the role of voxel size in determining leaf area distribution of forests with terrestrial LiDAR," *Agricultural and Forest Meteorology,* vol. 184, pp. 82-97, 2014.

[8] J. M. Norman, and J. M. Welles, "Radiative Transfer in an Array of Canopies 1," *Agronomy Journal,* vol. 75, no. 3, pp. 481-488, 1983.

[9] G. P. Asner, J. M. Scurlock, and J. A. Hicke, "Global synthesis of leaf area index observations: implications for ecological and remote sensing studies," *Global ecology and biogeography,* vol. 12, no. 3, pp. 191-205, 2003.

[10] J. M. Chen, and T. A. Black, "Defining leaf area index for non-flat leaves," *Plant, Cell and Environment,* vol. 15, no. 4, pp. 421-429, 1992.

[11] G. Yan, R. Hu, J. Luo, M. Weiss, H. Jiang, X. Mu, D. Xie, and W. Zhang, "Review of indirect optical measurements of leaf area index: Recent advances, challenges, and perspectives," *Agricultural and Forest Meteorology,* vol. 265, pp. 390-411, 2019/02/15/, 2019.

[12] N. J. Breda, "Ground-based measurements of leaf area index: a review of methods, instruments and current controversies," *J Exp Bot,* vol. 54, no. 392, pp. 2403-17, Nov, 2003.

[13] H. Fang, F. Baret, S. Plummer, and G. Schaepman-Strub, "An Overview of Global Leaf Area Index (LAI): Methods, Products, Validation, and Applications," *Reviews of Geophysics,* vol. 57, no. 3, pp. 739-799, 2019.

[14] Z. Liu, J. M. Chen, G. Jin, and Y. Qi, "Estimating seasonal variations of leaf area index using litterfall collection and optical methods in four mixed evergreen–deciduous forests," *Agricultural and Forest Meteorology,* vol. 209-210, pp. 36-48, 2015.

[15] J. W. Chason, D. D. Baldocchi, and M. A. Huston, "A comparison of direct and indirect methods for estimating forest canopy leaf area," *Agricultural and Forest Meteorology,* vol. 57, no. 1-3, pp. 107-128, 1991.

[16] I. Jonckheere, S. Fleck, K. Nackaerts, B. Muys, P. Coppin, M. Weiss, and F. Baret, "Review of methods for in situ leaf area index determination: Part I. Theories, sensors and hemispherical photography," *Agricultural and forest meteorology,* vol. 121, no. 1-2, pp. 19-35, 2004.

[17] J. W. Wilson, "Analysis of the Spatial Distribution of Foliage by Two-Dimensional Point Quadrats," *New Phytologist,* vol. 58, no. 1, pp. 92-99, 1959.

[18] J. Ross, *The radiation regime and architecture of plant stands*: Springer Science & Business Media, 1981.

[19] N. Taib, Z. Ali, A. Abdullah, F. S. Yeok, and R. Prihatmanti, "The performance of different ornamental plant species in transitional spaces in urban high-rise settings," *Urban Forestry & Urban Greening,* vol. 43, pp. 126393, 2019.

[20] L. F. Ow, S. Ghosh, and M. L. M. Yusof, "Growth of Samanea saman: Estimated cooling potential of this tree in an urban environment," *Urban Forestry & Urban Greening,* vol. 41, pp. 264-271, 2019.
[21] J. Klingberg, J. Konarska, F. Lindberg, L. Johansson, and S. Thorsson, "Mapping leaf area of urban greenery using aerial LiDAR and ground-based measurements in Gothenburg, Sweden," *Urban Forestry & Urban Greening,* vol. 26, pp. 31-40, 2017.
[22] F. Chianucci, N. Puletti, E. Giacomello, A. Cutini, and P. Corona, "Estimation of leaf area index in isolated trees with digital photography and its application to urban forestry," *Urban Forestry & Urban Greening,* vol. 14, no. 2, pp. 377-382, 2015.
[23] M. Alonzo, B. Bookhagen, J. P. McFadden, A. Sun, and D. A. Roberts, "Mapping urban forest leaf area index with airborne lidar using penetration metrics and allometry," *Remote Sensing of Environment,* vol. 162, pp. 141-153, 2015.
[24] T. E. Morakinyo, K. K.-L. Lau, C. Ren, and E. Ng, "Performance of Hong Kong's common trees species for outdoor temperature regulation, thermal comfort and energy saving," *Building and Environment,* vol. 137, pp. 157-170, 2018.
[25] M. A. Rahman, A. Moser, A. Gold, T. Rotzer, and S. Pauleit, "Vertical air temperature gradients under the shade of two contrasting urban tree species during different types of summer days," *Sci Total Environ,* vol. 633, pp. 100-111, Aug 15, 2018.
[26] M. Bouvier, S. Durrieu, R. A. Fournier, and J.-P. Renaud, "Generalizing predictive models of forest inventory attributes using an area-based approach with airborne LiDAR data," *Remote Sensing of Environment,* vol. 156, pp. 322-334, 2015.
[27] K. Liu, X. Shen, L. Cao, G. Wang, and F. Cao, "Estimating forest structural attributes using UAV-LiDAR data in Ginkgo plantations," *ISPRS Journal of Photogrammetry and Remote Sensing,* vol. 146, pp. 465-482, 2018.
[28] L. Cao, N. C. Coops, J. L. Innes, S. R. J. Sheppard, L. Y. Fu, H. H. Ruan, and G. H. She, "Estimation of forest biomass dynamics in subtropical forests using multi-temporal airborne LiDAR data," *Remote Sensing of Environment,* vol. 178, pp. 158-171, Jun 1, 2016.
[29] L. Cao, N. C. Coops, Y. Sun, H. H. Ruan, G. B. Wang, J. S. Dai, and G. H. She, "Estimating canopy structure and biomass in bamboo forests using airborne LiDAR data," *Isprs Journal of Photogrammetry and Remote Sensing,* vol. 148, pp. 114-129, Feb, 2019.
[30] T. Yun, K. Jiang, G. C. Li, M. P. Eichhorn, J. C. Fan, F. Z. Liu, B. Q. Chen, F. An, and L. Cao, "Individual tree crown segmentation from airborne LiDAR data using a novel Gaussian filter and energy function minimization-based approach," *Remote Sensing of Environment,* vol. 256, pp. 112307, Apr, 2021.
[31] D. Wu, S. Phinn, K. Johansen, A. Robson, J. Muir, and C. Searle, "Estimating Changes in Leaf Area, Leaf Area Density, and Vertical Leaf Area Profile for Mango, Avocado, and Macadamia Tree Crowns Using Terrestrial Laser Scanning," *Remote Sensing,* vol. 10, no. 11, pp. 1750, 2018.
[32] R. Hu, E. Bournez, S. Cheng, H. Jiang, F. Nerry, T. Landes, M. Saudreau, P. Kastendeuch, G. Najjar, J. Colin, and G. Yan, "Estimating the leaf area of an individual tree in urban areas using terrestrial laser scanner and path length distribution model," *ISPRS Journal of Photogrammetry and Remote Sensing,* vol. 144, pp. 357-368, 2018.
[33] S. D. Roberts, T. J. Dean, D. L. Evans, J. W. McCombs, R. L. Harrington, and P. A. Glass, "Estimating individual tree leaf area in loblolly pine plantations using LiDAR-derived measurements of height and crown dimensions," *Forest Ecology and Management,* vol. 213, no. 1-3, pp. 54-70, 2005.
[34] P. J. Olsoy, J. J. Mitchell, D. F. Levia, P. E. Clark, and N. F. Glenn, "Estimation of big sagebrush leaf area index with terrestrial laser scanning," *Ecological Indicators,* vol. 61, pp. 815-821, 2016.
[35] T. Yun, F. An, W. Li, Y. Sun, L. Cao, and L. Xue, "A Novel Approach for Retrieving Tree Leaf Area from Ground-Based LiDAR," *Remote Sensing,* vol. 8, no. 11, pp. 942, Nov, 2016.
[36] T. Yun, L. Cao, F. An, B. Chen, L. Xue, W. Li, S. Pincebourde, M. J. Smith, and M. P. Eichhorn, "Simulation of multi-platform LiDAR for assessing total leaf area in tree crowns," *Agricultural and Forest Meteorology,* vol. 276-277, 2019.
[37] L. Ma, G. Zheng, J. U. Eitel, T. S. Magney, and L. M. Moskal, "Determining woody-to-total area ratio using terrestrial laser scanning (TLS)," *Agricultural and forest meteorology,* vol. 228, pp. 217-228, 2016.
[38] F. Hosoi, and K. Omasa, "Voxel-Based 3-D Modeling of Individual Trees for Estimating Leaf Area Density Using High-Resolution Portable Scanning Lidar," *IEEE Transactions on Geoscience and Remote Sensing,* vol. 44, no. 12, pp. 3610-3618, 2006.
[39] F. Hosoi, Y. Nakai, and K. Omasa, "Estimation and Error Analysis of Woody Canopy Leaf Area Density Profiles Using 3-D Airborne and Ground-Based Scanning Lidar Remote-Sensing Techniques," *IEEE Transactions on Geoscience and Remote Sensing,* vol. 48, no. 5, pp. 2215-2223, 2010.
[40] M. Béland, J.-L. Widlowski, R. A. Fournier, J.-F. Côté, and M. M. Verstraete, "Estimating leaf area distribution in savanna trees from terrestrial LiDAR measurements," *Agricultural and Forest Meteorology,* vol. 151, no. 9, pp. 1252-1266, 2011.
[41] F. Pimont, D. Allard, M. Soma, and J.-L. Dupuy, "Estimators and confidence intervals for plant area density at voxel scale with T-LiDAR," *Remote Sensing of Environment,* vol. 215, pp. 343-370, 2018.
[42] V.-T. Nguyen, R. A. Fournier, J.-F. Côté, and F. Pimont, "Estimation of vertical plant area density from single return terrestrial laser scanning point clouds acquired in forest environments," *Remote Sensing of Environment,* vol. 279, pp. 113115, 2022.
[43] E. Grau, S. Durrieu, R. Fournier, J.-P. Gastellu-Etchegorry, and T. Yin, "Estimation of 3D vegetation density with Terrestrial Laser Scanning data using voxels. A sensitivity analysis of influencing parameters," *Remote Sensing of Environment,* vol. 191, pp. 373-388, 2017.
[44] M. Soma, F. Pimont, and J.-L. Dupuy, "Sensitivity of voxel-based estimations of leaf area density with terrestrial LiDAR to vegetation structure and sampling limitations: A simulation experiment," *Remote Sensing of Environment,* vol. 257, pp. 112354, 2021.
[45] M. Soma, F. Pimont, D. Allard, R. Fournier, and J.-L. Dupuy, "Mitigating occlusion effects in Leaf Area Density estimates from Terrestrial LiDAR through a specific kriging method," *Remote Sensing of Environment,* vol. 245, pp. 111836, 2020.
[46] S. Hancock, K. Anderson, M. Disney, and K. J. Gaston, "Measurement of fine-spatial-resolution 3D vegetation structure with airborne waveform lidar: Calibration and validation with voxelised terrestrial lidar," *Remote Sensing of Environment,* vol. 188, pp. 37-50, 2017.
[47] Y. Li, Q. Guo, Y. Su, S. Tao, K. Zhao, and G. Xu, "Retrieving the gap fraction, element clumping index, and leaf area index of individual trees using single-scan data from a terrestrial laser scanner," *ISPRS Journal of Photogrammetry and Remote Sensing,* vol. 130, pp. 308-316, 2017.
[48] N. F. Sirri, M. B. Libalah, S. Momo Takoudjou, P. Ploton, V. Medjibe, N. G. Kamdem, G. Mofack, B. Sonké, and N. Barbier, "Allometric Models to Estimate Leaf Area for Tropical African Broadleaved Forests," *Geophysical Research Letters,* vol. 46, no. 15, pp. 8985-8994, 2019.
[49] D. Xie, Y. Wang, R. Hu, Y. Chen, G. Yan, W. Zhang, and P. Wang, "Modified gap fraction model of individual trees for estimating leaf area using terrestrial laser scanner," *Journal of Applied Remote Sensing,* vol. 11, no. 3, pp. 035012, 2017.
[50] Y. Lin, and G. West, "Retrieval of effective leaf area index (LAIe) and leaf area density (LAD) profile at individual tree level using high density multi-return airborne LiDAR," *International Journal of Applied Earth Observation and Geoinformation,* vol. 50, pp. 150-158, 2016.
[51] I. Moorthy, J. R. Miller, B. Hu, J. Chen, and Q. Li, "Retrieving crown leaf area index from an individual tree using ground-based lidar data," *Canadian Journal of Remote Sensing,* vol. 34, no. 3, pp. 320-332, 2008.
[52] A. Lang, and X. Yueqin, "Estimation of leaf area index from transmission of direct sunlight in discontinuous canopies," *Agricultural and forest Meteorology,* vol. 37, no. 3, pp. 229-243, 1986.
[53] J. M. Chen, and J. Cihlar, "Plant canopy gap-size analysis theory for improving optical measurements of leaf-area index," *Appl Opt,* vol. 34, no. 27, pp. 6211-22, Sep 20, 1995.
[54] S. G. Leblanc, J. M. Chen, R. Fernandes, D. W. Deering, and A. Conley, "Methodology comparison for canopy structure parameters extraction from digital hemispherical photography in boreal forests," *Agricultural and Forest Meteorology,* vol. 129, no. 3-4, pp. 187-207, 2005.
[55] R. Hu, G. Yan, X. Mu, and J. Luo, "Indirect measurement of leaf area index on the basis of path length distribution," *Remote Sensing of Environment,* vol. 155, pp. 239-247, 2014.
[56] X. Zhu, A. K. Skidmore, T. Wang, J. Liu, R. Darvishzadeh, Y. Shi, J. Premier, and M. Heurich, "Improving leaf area index (LAI) estimation by correcting for clumping and woody effects using terrestrial laser scanning," *Agricultural and Forest Meteorology,* vol. 263, pp. 276-286, 2018.
[57] Y. Chen, W. Zhang, R. Hu, J. Qi, J. Shao, D. Li, P. Wan, C. Qiao, A. Shen, and G. Yan, "Estimation of forest leaf area index using terrestrial laser scanning data and path length distribution model in open-canopy

forests," *Agricultural and Forest Meteorology,* vol. 263, pp. 323-333, 2018.

[58] Y. Lai, X. Mu, W. Li, J. Zou, Y. Bian, K. Zhou, R. Hu, L. Li, D. Xie, and G. Yan, "Correcting for the clumping effect in leaf area index calculations using one-dimensional fractal dimension," *Remote Sensing of Environment,* vol. 281, 2022.

[59] G. Sonohat, H. Sinoquet, V. Kulandaivelu, D. Combes, and F. Lescourret, "Three-dimensional reconstruction of partially 3D-digitized peach tree canopies," *Tree Physiol,* vol. 26, no. 3, pp. 337-51, Mar, 2006.

[60] R. Ceulemans, J. Y. Pontailler, F. Mau, J. Guittet, and B. Legay, "Leaf Allometry in Young Poplar Stands - Reliability of Leaf-Area Index Estimation, Site and Clone Effects," *Biomass & Bioenergy,* vol. 4, no. 5, pp. 315-321, 1993.

[61] E. Bournez, T. Landes, G. Najjar, P. Kastendeuch, J. Ngao, and M. Saudreau, "Sensitivity of simulated light interception and tree transpiration to the level of detail of 3D tree reconstructions," *Urban Forestry & Urban Greening,* vol. 38, pp. 1-10, 2019.

[62] PCM, ": PointCloud Magic. 2.0.0. November 2020. PCM Development Core Team. http://www.lidarcas.cn/soft.20201206."

[63] G. Yan, H. Jiang, J. Luo, X. Mu, F. Li, J. Qi, R. Hu, D. Xie, and G. Zhou, "Quantitative Evaluation of Leaf Inclination Angle Distribution on Leaf Area Index Retrieval of Coniferous Canopies," *Journal of Remote Sensing,* vol. 2021, 2021.

[64] S. Leblanc, "Tracing radiation and architecture of canopies. trac manual, version 2.1," *Natural Resources Canada,* vol. 2, pp. 1-25, 2002.

[65] S. Tao, F. Wu, Q. Guo, Y. Wang, W. Li, B. Xue, X. Hu, P. Li, D. Tian, C. Li, H. Yao, Y. Li, G. Xu, and J. Fang, "Segmenting tree crowns from terrestrial and mobile LiDAR data by exploring ecological theories," *ISPRS Journal of Photogrammetry and Remote Sensing,* vol. 110, pp. 66-76, 2015.

[66] H. Edelsbrunner, and E. P. Mücke, "Three-dimensional alpha shapes," *ACM Transactions on Graphics,* vol. 13, no. 1, pp. 43-72, 1994.

[67] M. D. Baptista, S. J. Livesley, E. G. Parmehr, M. Neave, and M. Amati, "Variation in leaf area density drives the rainfall storage capacity of individual urban tree species," *Hydrological Processes,* vol. 32, no. 25, pp. 3729-3740, 2018.

[68] McPherson, E. Gregory; van Doorn, Natalie S.; Peper, Paula J. 2016. Urban tree database. Fort Collins, CO: Forest Service Research Data Archive. Updated 21 January 2020. https://doi.org/10.2737/RDS-2016-0005.

[69] E. G. McPherson, N. S. van Doorn, and P. J. Peper, *Urban tree database and allometric equations*: US Department of Agriculture, Forest Service, Pacific Southwest Research …, 2016.

[70] N. Otsu, "A threshold selection method from gray-level histograms," *IEEE transactions on systems, man, and cybernetics,* vol. 9, no. 1, pp. 62-66, 1979.